

DAReN: A Collaborative Approach Towards Visual Reasoning And Disentangling

Prithish Sahu, Kalliopi Basioti, Vladimir Pavlovic

Department of Computer Science, Rutgers University

{prithish.sahu, kalliopi.basioti}@rutgers.edu, vladimir@cs.rutgers.edu

Abstract—Computational learning approaches to solving visual reasoning tests, such as Raven’s Progressive Matrices (RPM), critically depend on the ability to identify the visual concepts used in the test (i.e., the representation) as well as the latent rules based on those concepts (i.e., the reasoning). However, learning of representation and reasoning is a challenging and ill-posed task, often approached in a stage-wise manner (first representation, then reasoning). In this work, we propose an end-to-end joint representation-reasoning learning framework, which leverages a weak form of inductive bias to improve both tasks together. Specifically, we introduce a general generative graphical model for RPMs, *GM-RPM*, and apply it to solve the reasoning test. We accomplish this using a novel learning framework Disentangling based Abstract Reasoning Network (DAReN) based on the principles of *GM-RPM*. We perform an empirical evaluation of DAReN over several benchmark datasets. DAReN shows consistent improvement over state-of-the-art (SOTA) models on both the reasoning and the disentanglement tasks. This demonstrates the strong correlation between disentangled latent representation and the ability to solve abstract visual reasoning tasks.

I. INTRODUCTION

Raven’s Progressive Matrices (RPM) [1], [2], [3] is a widely acknowledged metric in the research community to test the cognitive skills of humans. RPM is primarily used to assess lateral thinking, i.e., the ability to systematically process the results and find solutions to unseen problems without drawing on prior knowledge [4]. The vision community has often employed Raven’s test to evaluate the abstract reasoning skills of an AI model [5], [6], [7], [8], [9]. Figure 1 illustrates a RPM question, given a 3×3 matrix, where each cell contains a visual geometric design except for the last cell in the bottom row. An AI model must pick the best-fit image from a list of six to eight choices to complete the matrix. Solving the question requires figuring out the underlying rules in the matrix as shown in Figure 1 where the correct rule is “color is constant in a row”, which eliminates other choices leaving choice “A” as the correct answer. An AI model needs to infer the underlying rules in the top two rows or columns to fill the missing piece in the last row. The visual IQ score of the above model obtained via solving abstract reasoning tasks can provide ground to compare AI against human intelligence.

Earlier computation models depended on handcrafted heuristics rules on propositions formed from visual inputs to solve RPM [10], [11]. The lack of success in the previous approaches and the inclusion of large RPM datasets [12], PGM [13], RAVEN [14] facilitated the employment of neural networks to solve abstract reasoning tasks [5], [13],

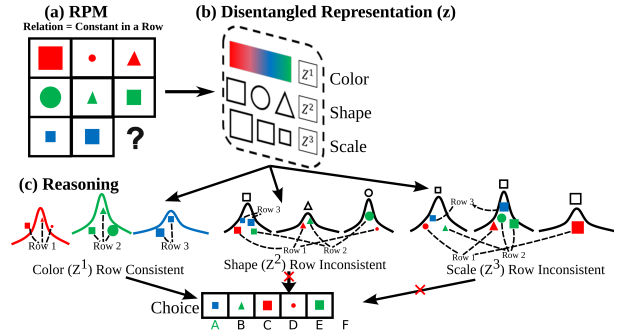


Fig. 1: **a:** RPM instance with rule “constant-in-a-row”. **b.** The true generative factors in the data. **c. Reasoning with factors:** The distribution of z^i is represented by a Gaussian. Only z^1 (color) satisfies the rule while the other two factors are inconsistent. **Index one** in the choice list is the correct answer.

[14], [12], [15]. Until now, these abstract reasoning methods have employed existing deep learning methods such as CNN [16], ResNet [17] to improve reasoning but largely ignore to learn the visual attributes as independent components. Even though these models have improved abstract reasoning tasks, the performance is still sub-optimal compared to humans. These setbacks to the model performance are caused due to the lack of adequate and task-appropriate visual representation. The model should learn to separate the key attributes needed for reasoning as independent components.

These critical attributes, aka disentangled representations, [18], [19] break down the visual features to their independent generative factors, capable of generating the full spectrum of variations in the ambient data. We argue that a better-disentangled model is essential for the better reasoning ability of machines. A recent study [20] via impossibility theorem has shown the limitation of learning disentanglement independently. The impossibility theorem states that without any form of inductive bias, learning disentangled factors is impossible. Since collecting label information of the generative factors is challenging and almost impossible in real-world datasets, previous works have focused on some form of semi-supervised or weakly-supervised methods. Few of the prior works in disentanglement using inductive bias involve [21] that uses a subset of ground truth factors, [22] that formed pair of images with common visual attributes on a subset of factors, and [23] where the factors in a pair of images are ranked on the subset of factors. Our work improves upon the model’s reasoning ability by using the inductive reasoning present in the spatial

features. Utilizing the underlying reasoning, i.e., rules on visual attributes in RPM induces weak supervision that helps improve disentanglement, leading to better reasoning.

[12] investigated the dependency between ground truth factor of variations and reasoning performance. We take a step further and consider jointly learning disentangled representation and learning to reason (critical thinking). Unlike the above-proposed model, i.e. (working in a staged process to improve disentangling or improve downstream accuracy), we work on the weakness of both components and propose a novel way to optimize both in a single end-to-end trained model. We demonstrate the benefits of the interaction between representation learning and reasoning ability. Our motivation behind using the same evaluation procedure by [12] is as follows: 1) the strong visual presence, 2) information of the generative factors help in demonstrating the model efficacy on both reasoning accuracy and disentanglement (strong correlation), 3) possibility of comparing the disentangled results with state-of-the-art disentangling results.

In summary, the contributions of our work are threefold: (1) We propose a general generative graphical model for RPM, GM-RPM, which will form the essential basis for inductive bias in joint learning for representation + reasoning. (2) Building upon GM-RPM, we propose a novel learning framework named **Disentangling based Abstract Reasoning Network (DAReN)** composed of two primary components – disentanglement network, and reasoning network. It learns to disentangle factors and uses the representation to detect the underlying relationship and the object property used for the relation. To our knowledge, (DAReN) is the first joint learning framework that separates the underlying generative factors and solve reasoning. (3) We show that DAReN outperforms all state-of-the-art baseline models in reasoning and disentanglement metrics, demonstrating that reasoning and disentangled representations are tightly related; learning both in unison can effectively improve the downstream reasoning task.

II. RELATED WORKS

Visual Reasoning. Solving RPM have recently gained much attention due to their high correlation with human intelligence [3], [13], [14]. Initial works based on rule-based heuristics such as symbolic representations [1], [7], [8], [9] or relational structures [6], [24], [25] failed to comprehend the reasoning tasks due to their underlying assumptions. These assumptions include access to the symbolic representations of images, domain expertise on the underlying operations, and comparisons that help solve the task. [26] proposed a systematic way of automatically generating RPM using first-order logic to try to understand and solve these tasks fully. Growing interest introduced two RPM dataset [13], [14], which led to significant progress in solving reasoning tasks [27], [28], [5], [13].

Disentanglement. Recovering independent data generating ground truth factors is a well-studied problem in machine learning. In recent years there is renewed interest in unsupervised learning of disentangled representations [29], [30], [31],

[32], [20], [19], [33]. Nevertheless, this research area has not reached a major consensus on two major notions: i) no widely accepted formalized definition [18], [19], [20], [33], ii) no single robust evaluations metrics to compare the models [34], [30], [35], [36], [37]. However, the key fact common in all models is the recovery of statistically independent [19] learned factors. A majority of the research follows the definition presented in [18], which states that the underlying generative factors correspond to independent latent dimensions, such that changing a single factor of variation should change only a single latent dimension while remaining invariant to others. Recent work [20] showed that it is impossible to learn disentangled representation without the presence of inductive bias, prompting the shift to semi-supervised [38], [39], [40] and weak-supervised [41], [22], [42], [43] disentangling models.

Recent reasoning works [27], [28] have focused on Raven [14], PGM [13] datasets for evaluation. In contrast to the above, we focus on learning both disentangled representation and solving abstract visual reasoning. Our work is inspired by the large-scale study in [12], suggesting dependence between learning disentangled representations and solving visual reasoning. Our proposed framework leverages joint learning, which improves both the reasoning and the disentanglement performance. Since we quantify disentanglement score along with reasoning accuracy, the datasets used in [12] are well suited compared to Raven [14], PGM [13] which are not adapted for quantitative evaluation of disentanglement.

III. PROBLEM FORMULATION AND APPROACH

We begin by describing the problem of RPM in the domain of visual reasoning task in Section III-A, where we elaborate on the process of what constitutes valid RPM. Next, we propose our general generative graphical model for RPM, *GM-RPM*, which will form the essential basis for inductive bias in joint learning for representation and reasoning in Section III-B. Finally, in Section III-C, we describe our learning framework a.k.a **Disentangling based Abstract Reasoning Network (DAReN)** based on a variational autoencoder (VAE) and a reasoning network for joint representation-reasoning learning.

A. Visual Reasoning Task

The Raven’s matrix denoted as \mathcal{M} , of size $M \times M$ contains images at all i, j location except at \mathcal{M}_{MM} . The aim is to find the best fit image a^* at \mathcal{M}_{MM} from a list of choices denoted as A . For our current work, we follow the procedure by [12] to prepare RPM. Similar to prior work, we have fixed $M = 3$, where $\mathcal{M} = \{x_{11}, \dots, x_{32}\}$ in row-major order and \mathcal{M}_{33} is empty that needs to be placed with the correct image from the choices. We also set the number of choices $|A| = 6$, where $A = \{a_1, \dots, a_6\}$. We improve upon the prior work by formulating an abstract representation for the matrices \mathcal{M} by defining a structure S on the image attributes (o) and relation types (r) applied to the image attributes:

$$S = \{(r, o) : r \in R \text{ and } o \in O\}.$$

The set R consists of relations proposed by [1] that are constant in a row, quantitative pairwise progression, figure addition or subtraction, distribution of three values, and distribution of two values. We assume images are generated from underlying ground truth data generative factors (K) that constitute RPM. These image factors (O) consist of the object type, size, position (XY-axis), and color. The structure S is a set of tuples, where each tuple is formed by randomly sampling a relation from R and image attribute from O . For instance, if $S = \{(\text{constant in a row, color}), (\text{quantitative pairwise progression, size})\}$, every image in each row of \mathcal{M} will have the same (constant) value for attribute color, and progression relation instantiated on size of images from left to right. This set of S can contain a max of $|R| * |O|$ tuple, where the problem difficulty rises with the increase in the size of R , O or $|S|$ or any combination of them.

Generating RPM. Using S , multiple realizations of the matrix \mathcal{M} are possible depending on the randomly sampled values of (r, o) . We use o to denote the image attributes in S , in the example above $S = \{\text{color, object type}\}$ ¹. In the generation process, we sample values for attributes in o that adhere to their associated relation r and the values for image attributes in $\bar{o} = O \setminus o$, that are not part of S , are sampled randomly for every image. Next, we sample images at every \mathcal{M}_{ij} where the image attribute values matches with the values sampled above for $o \cup \bar{o}$. For the matrix \mathcal{M} to be a valid RPM the sampled values for \bar{o} must not comply with the relation set $r \in S$ across all rows in \mathcal{M} . However, in the above example where $\bar{o} = \{\text{position, size}\}$, a valid \mathcal{M} can also have the same values for position or size (or both) in a row as long as they do not adhere to any relations in S for more than one row. The above is an example of a distractor, where the attributes in \bar{o} during the sampling process might satisfy some $(r, o) \in S$ for any one row in \mathcal{M} but not for all M rows. These randomly varying values in \bar{o} add a layer of difficulty towards solving RPM. The result of the above generation steps produces a valid RPM matrix \mathcal{M} . The task of any model trained to solve \mathcal{M} has to find r that is consistent across all rows or columns in o and discard the distracting features \bar{o} . In the rest of the paper, we focus on the row-based relationship in RPM².

B. Inductive Prior for RPM (GM-RPM)

While previous works have made strides in solving RPM [6], [7], [12], the gap in reasoning and representation learning between those approaches and the human performance remains. To narrow this gap, we propose a minimal inductive bias in the form of a probabilistic graphical model described here that can be used to guide the joint representation-reasoning learning. Figure 2 defines the structure of the general generative graphical model for RPM. This model describes an RPM $\mathcal{M} = \{x_{11}, \dots, x_{MM}\}$, where $x_{ij}, i, j = 1, \dots, M$,

¹We interchangeably use o to denote the subset of image attributes that adhere to rules of RPM as well as the multi-hot vector $o \in \{0, 1\}^K$ whose non-zero values index those attributes.

²Our solution could trivially be extended to address columns or both rows and columns.

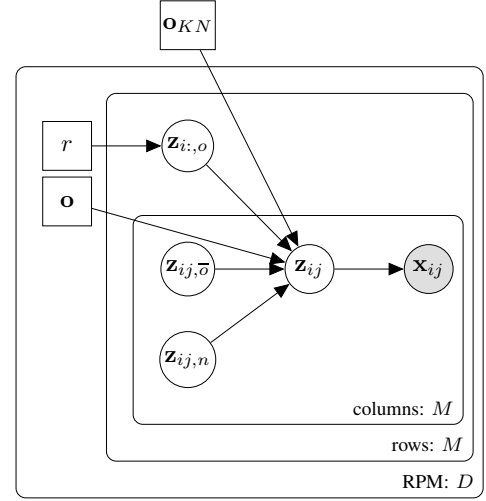


Fig. 2: Generative model for RPM. See Sec. III-B for details.

denote the images in the puzzle, with the correct answer at x_{MM} , defined by rule r and factors o .

Latent vectors $z_{ij} \in \mathbb{R}^{K+N}$ are the representations of the K attributes, to be learned by our approach, and some inherent noise process encompassed in the remaining N dimensions of z_{ij} , $z_{ij,n} \in \mathbb{R}^N$, which we refer to as nuisances. Ideally, some K factors in z_{ij} should be isomorphic to the attributes themselves in this simple RPM setting, after an optimal model is learned. We index those K relevant factors with a hierarchical indexing model, illustrated in Figure 3.

The latent attribute selection vector $o \in \{0, 1\}^K$ determines which, among the K possible, factors are used in the puzzle. This vector is embedded over a larger attribute-noise selection vector $o_{KN} \in \{0, 1\}^{K+N}$. In $o_{KN,j} = 0$, $j = K+1, \dots, K+N$ indicate the factors corresponding to nuisance, determination of which is a part of the inference process, as defined below in (2).

This latent vector gives rise to ambient images through some stochastic nonlinear mapping $x \sim p(x|f(z|\Theta))$ ³, where $Z = [z_{ij}]_{M \times M} \in \mathbb{R}^{M \times M \times (K+N)}$ is the mapped latent tensor for RPM, parameterized by Θ which is to be learned,

$$p(\mathcal{M}|Z, \Theta) = \prod_i \prod_j p(x_{ij}|f(z_{ij}|\Theta)), \quad (1)$$

The RPM inductive bias comes from the way (prior) z_{ij} are formed, given the unknown rule r . Specifically,

$$z_{ij} = o_{KN} \odot \begin{bmatrix} o \odot z_{ij,o} + \bar{o} \odot z_{ij,\bar{o}} \\ \mathbf{0}_N \end{bmatrix} + \bar{o}_{KN} \odot \begin{bmatrix} \mathbf{0}_K \\ z_{ij,n} \end{bmatrix}, \quad (2)$$

³We drop RPM indices, where obvious.

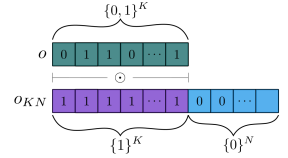


Fig. 3: Illustration of the indexing vectors o and o_{KN} . ‘1’ entries in o indicate the relevant factors used in a puzzle instance. N ‘0’ entries (blue) in o_{KN} correspond to nuisance factors, which are not used in any puzzle instances.

where $\mathbf{z}_{ij,o} \in \mathbb{R}^K$ is the latent representation of the factors that are used in rule r , $\mathbf{z}_{ij,\bar{o}} \in \mathbb{R}^K$ is the latent representation of the complementary, unused factors⁴.

The key in RPM is to define the priors on factors. The factors used in the rule, grouped as the tensor $\mathbf{Z}_o = [\mathbf{z}_{ij,o}]_{M \times M}$, follow a joint density over $j = 1, \dots, M$ in row i

$$p(\mathbf{Z}_o|r) = \prod_i p(\mathbf{z}_{i,:}|r) = \prod_i p(\mathbf{z}_{i1,o}, \dots, \mathbf{z}_{iM,o}|r), \quad (3)$$

where $\mathbf{z}_{i,:}$ is the matrix of size $K \times M$ or all latent representations in row i of RPM. The factors *not* used in the rule, \bar{o} , and actors representing the noise information have a different, iid prior (refer inner-most plate, “columns: M ”, in Figure 2)

$$p(\mathbf{Z}_{\bar{o}}|r) = \prod_i \prod_j p(\mathbf{z}_{ij,\bar{o}}), \quad p(\mathbf{Z}_n) = \prod_m \prod_j \mathcal{N}(\mathbf{z}_{mj,n}; 0, I) \quad (4)$$

We assume that all $K + N$ factors are independent,

$$p(\mathbf{z}_{i:,o}|r) = \prod_k p(\mathbf{z}_{i:,o}^k|r), \quad p(\mathbf{z}_{ij,\bar{o}}) = \prod_k p(\mathbf{z}_{ij,\bar{o}}^k) \\ p(\mathbf{z}_{ij,n}) = \prod_k p(\mathbf{z}_{ij,n}^k).$$

This gives rise to the full Generative Models (**GM-RPM**),

$$P(\mathcal{M}; \mathbf{Z}, \mathbf{Z}_o, \mathbf{Z}_{\bar{o}}, \mathbf{Z}_n, r, \mathbf{o}, \mathbf{o}_{KN}) = \\ p(\mathcal{M}|\mathbf{Z})p(\mathbf{Z}|\mathbf{Z}_o, \mathbf{Z}_{\bar{o}}, \mathbf{Z}_n, \mathbf{o}, \mathbf{o}_{KN})p(\mathbf{Z}_o|r)p(\mathbf{Z}_{\bar{o}})p(\mathbf{Z}_n). \quad (5)$$

Inference Model. As described in Section III-B, the goal is to infer the value of the latent variables that generated the observations, i.e., to calculate the posterior distribution over $p(\mathbf{Z}, \mathbf{o}, r|\mathcal{M})$, which is intractable. Instead, an approximate solution for the intractable posterior was proposed by [44] that uses a variational approximation $q(\mathbf{Z}, \mathbf{o}, r|\mathcal{M}; \phi)$, where ϕ are the variational parameters. In this work, we further define this variational posterior as

$$q(\mathbf{Z}, \mathbf{o}, \mathbf{o}_{KN}, r|\mathcal{M}; \phi) \propto q_Z(\mathbf{Z}|\mathbf{Z}', r, \mathbf{o}, \mathbf{o}_{KN})q_r(r|\mathbf{Z}', \mathbf{o}) \\ q_o(\mathbf{o}|\mathbf{o}_{KN}, \mathbf{Z}')q_{\bar{o}}(\mathbf{o}_{KN}|\mathbf{Z}') \prod_{ij} q_{\phi}(\mathbf{z}_{ij}'|\mathbf{x}_{ij}), \quad (6)$$

where \mathbf{Z}' is an intermediate variable which is used to arrive at the final estimate of \mathbf{Z} using the Factor Consistency inference as described further in this section.

Currently, DAREn is designed for $r = \text{“constant-in-a-row”}$, i.e., $q_r(r|\mathbf{Z}', \mathbf{o}) = \delta(r - r_{const})$ from (6). Next, we describe the sequential inference process for all the latents.

Infer \mathbf{Z}' : Intermediate latent factors \mathbf{Z}' are first inferred independently for each element \mathbf{x}_{ij} using a general stochastic encoder q_{ϕ} of the VAE family:

$$q_{\phi}(\mathbf{Z}'|\mathcal{M}) = \prod_{ij} q_{\phi}(\mathbf{z}_{ij}'|\mathbf{x}_{ij}). \quad (7)$$

Our framework accepts arbitrary choices of the VAE-family encoders, as discussed in Sec. III-C.

Infer \mathbf{o}_{KN} : To infer K , we prune out the N nuisance attributes from $\mathbf{Z}' \in \mathbb{R}^{K+N}$ that have collapsed to the prior ($q_{\phi}(\mathbf{z}_{ij}'|\mathbf{x}_{ij}) = p(\mathbf{z}_{ij}')^*$). Thus the remaining latent dimensions form the relevant K attributes. This is similar to computing

the empirical variance $\mathbb{V}(\mathbf{Z}')$ to set the indices of \mathbf{o}_{KN} where the variance is above a threshold ($\epsilon = 0.05$).

$$q_o(\mathbf{o}_{KN}|\mathbf{Z}') = \delta(\mathbf{o}_{KN} - \hat{\mathbf{o}}_{KN}(\mathbf{Z}')) \quad (8)$$

$$\hat{\mathbf{o}}_{KN}(\mathbf{Z}') = \mathbb{1}_{\mathbb{V}(\mathbf{Z}') > \epsilon}^K, \quad (9)$$

where $\mathbb{1}_{a(x) \geq b}^K$ is the multi-hot indicator vector whose entries are set to 1 for the K largest values of $a(x)$ for which $a(x) \geq b$ holds. These K factors model the actual ground truth factors, while the remaining N factors $\mathbf{z}_{ij,n}'$ are considered nuisances.

Infer \mathbf{o} : Next, we use the multi-hot vector \mathbf{o}_{KN} to set only the selected attribute for the given instance of RPM. For a given \mathcal{M} and $r = \text{constant}$ in a row, $\mathbf{o}_{KN,i,:}$ values remains the same for images in row i . We utilize KL divergence as a measure over all pairwise \mathbf{z}_{ij}' , and set only on the indices with l -lowest divergence values to arrive at

$$q_o(\mathbf{o}|\mathbf{o}_{KN}, \mathbf{Z}') = \delta(\mathbf{o} - \hat{\mathbf{o}}(\mathbf{o}_{KN}, \mathbf{Z}')) \quad (10)$$

$$\hat{\mathbf{o}}(\mathbf{o}_{KN}, \mathbf{Z}') = \mathbb{1}_{-\delta_{KL}}^l \quad (11)$$

$$\delta_{KL}(k) = \frac{1}{M^3} \sum_{m,i,j=1}^M D_{KL}(q_{\phi}(\mathbf{z}_{ij}'|\mathbf{x}_{ij})||q_{\phi}(\mathbf{z}_{im}'|\mathbf{x}_{im})) \quad (12)$$

where, for $k = 1, \dots, K$.

Infer \mathbf{Z} using Factor Consistency: We describe the process of estimating \mathbf{Z} from the intermediate variable \mathbf{Z}' using $q_Z(\mathbf{Z}|\mathbf{Z}', r, \mathbf{o}, \mathbf{o}_{KN})$, for the chosen case of r ; the goal here is to obtain consistent, denoised final estimates of the factors, given the intermediate noisy estimates \mathbf{Z}' and the estimated relevant factors \mathbf{o} . Specifically,

$$\hat{\mathbf{z}}_{ij} = \hat{\mathbf{o}}_{KN} \odot \left[\hat{\mathbf{o}} \odot f_{avg}(\mathbf{z}_{i:,o}') + \hat{\bar{\mathbf{o}}} \odot \mathbf{z}_{ij,\bar{o}}' \right] + \hat{\bar{\mathbf{o}}}_{KN} \odot \left[\mathbf{0}_K \right]_{\mathbf{z}_{ij,n}'}, \quad (13)$$

and $q_Z(\mathbf{Z}|\mathbf{Z}', r, \mathbf{o}, \mathbf{o}_{KN}) = \delta(\hat{\mathbf{Z}} - \hat{\mathbf{Z}})$.

Since the relation r acts on the latent vector \mathbf{Z}_o , we apply the averaging strategy on it. For $r = r_{const}$, the averaging strategy is a variant of the method in Multi Level VAE [22] described for row i as:

$$f_{avg}(\mathbf{z}_{ij,o}') = \frac{1}{M} \sum_{j=1}^M \mathbf{z}_{ij,o}'. \quad (14)$$

Using (13) & (14), we obtain updated rule-attribute constrained latent representations \mathbf{Z} for each in \mathcal{M} . The resulting \mathbf{Z} is given as an input to the decoder network to learn to reconstruct the original Raven’s matrix, which we denote $\hat{\mathcal{M}}$.

C. DAREn

Inspired by *GM-RPM*, we propose a novel framework named Disentangling based Abstract Reasoning Network (DAREn). Please refer to Figure 4 for an overview of DAREn. DAREn is composed of two primary components, a variational auto encoder (VAE) module and a reasoning module. Using Section III-B described above our variational autoencoder (VAE) learns $q_{\phi}(\mathbf{Z}|\mathcal{M})$ (\mathbf{Z} is the final estimate) and $p_{\theta}(\mathcal{M}|\mathbf{Z})$, where the former is referred as encoder or inference model and the later as decoder or generative model. We assume that the factors vary independently, hence to drive to maximize statistical independence we append the VAE evidence lower bound objective with the Total Correlation (TC) term [30],

$$TC(\mathbf{Z}) = \prod_i \prod_j D_{KL}[q(\mathbf{z}_{ij})||\prod_l q(\mathbf{z}_{ij}^l)] \quad (15)$$

⁴We use $\mathbf{0}_l$ notation for a vector of all zeros of dimension l .

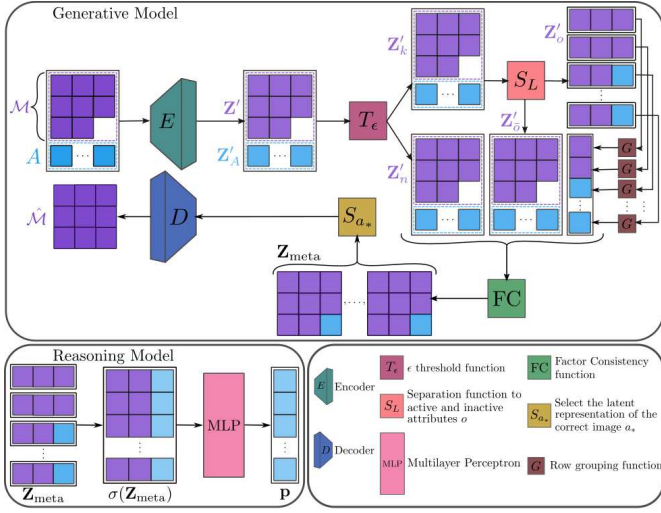


Fig. 4: Illustration of **DAREn**. It consists of a VAE-based generative and reasoning network. **Generative Model**. The encoder encodes \mathcal{M} and A to \mathbf{Z}' and \mathbf{Z}'_A . The K possible attributes are learned from \mathcal{M} by picking the factor indices with high variance, and the rest are kept as nuisances (N), performed by the threshold function T_ϵ . Next, with S_L , we further split the K -D latent representation to two groups of vectors \mathbf{Z}'_o and $\mathbf{Z}'_{\bar{o}}$ related to the active (set bits of o) and inactive (set bits of \bar{o}) attributes. No operation is performed on the factor indices at the set bit of \bar{o} and the nuisance factors. The rule constraint is enforced on the set bit of o to take the same value via an averaging strategy (G). The decoder receives the updated latent representation of the correct choice image a_* to reconstruct the image back ($\hat{\mathcal{M}}$). **Reasoning Model**. We consider the latent representation \mathbf{Z}_{meta} to extract the standard deviation across factor index for the top two rows and all possible six rows. An MLP trained on the concatenated standard deviation of the top two rows with choice a_i predicts the best fit image.

The form of the augmented ELBO objective is described as:

$$L_{\phi, \theta}(\mathcal{M}) = E_{p(\mathcal{M})}[E_{q_\phi(\mathbf{Z}_o|\mathcal{M}, r)}[q_\phi(\mathbf{Z}_{\bar{o}}|\mathcal{M}, r)] \log p_\theta(\mathcal{M}|\mathbf{Z})] - \lambda_1 [D_{KL}[q(\mathbf{Z}_o|\mathcal{M}, r)||p(\mathbf{Z}_o|r)] + D_{KL}[q(\mathbf{Z}_{\bar{o}}|\mathcal{M}, r)||p(\mathbf{Z}_{\bar{o}}|r)] + D_{KL}[q(\mathbf{Z}_n|\mathcal{M})||p(\mathbf{Z}_n)]] - \lambda_2 TC(\mathbf{Z}), \quad (16)$$

where hyperparameter λ_1, λ_2 controls the weight on the KL-divergence and the TC respectively.

Reasoning Module. The reasoning component of **DAREn** incorporates a relational structure to infer the abstract relationship on the attribute o for images in \mathcal{M} . The reasoning module receives disentangled representations, \mathbf{Z} (of \mathcal{M}) and \mathbf{Z}_A (of choices A). We prepare \mathbf{Z}_{meta} of size $(M+|A|-1) \times M$ by iteratively filling each choice as the missing piece.

Therefore, solving \mathcal{M} is equivalent to finding the correct row in $\{M, \dots, M+|A|-1\}$, that satisfies the same rules shared by the top $M-1$ rows. We compute the variance for all M representation in each row i , $\sigma(\mathbf{Z}_{\text{meta}(i)})$ over each dimension in the latent representation. The above process is applied to all the $M+|A|-1$ rows that include all $|A|$ probable last rows. Next, we concatenate the variance vector of the top $M-1$ rows with each probable last row (Figure 4) to prepare $|A|$ choice variance vectors, $\mathbb{R}^{|A| \times M \times (K+N)}$. We feed this concatenated variance vector to a three-layered MLP (ψ)

with a ReLU and a dropout layer [45], the probability of \bar{a} is estimated as:

$$p_i = \psi([\sigma(\mathbf{Z}_{\text{meta}(1)}) \cdots \sigma(\mathbf{Z}_{\text{meta}(M-1)}) \sigma(\mathbf{Z}_{\text{meta}(i)})]), \quad (17)$$

where $i \in \{M, \dots, (M+|A|-1)\}$ corresponds to $|A|$ probable choices. The choice with the highest score is predicted as the correct answer. The above process is trained using a Cross Entropy loss function.

IV. EXPERIMENTS

A. Datasets, Baselines, Experimental Setup

We study the performance of **DAREn** on six benchmark datasets used in disentangling work, (i) *dsprites* [46], (ii) modified *dSprites* [12], (iii) *shapes3d* [30], (iv-vi) MPI3D – (Real, Realistic, Toy) [47]. We use experimental settings similar to [12] to create RPM for the above datasets. The training procedure in [12], referred as *Staged-WReN*, is used as our baseline model. The *Staged-WReN* is a two-stage training process, where a disentangling generative network is first trained ($\sim 300K$ iterations), followed by training a Wild Relational Network (WReN) [13] on RPM using the representation (at $300K$) obtained from the trained encoder. Building on *Staged-WReN*, we propose an adapted baseline referred to as *E2E-WReN*, where we jointly train both the disentangling and the reasoning network from end-to-end. To train **DAREn**, we use a warm start by initializing only its VAE parameters with a partially trained Factor VAE [30] model for $\sim 100K$ on the above datasets (not RPM instances) followed by training **DAREn** for $200K$ iterations on the RPM generated from the datasets. We evaluate the model’s performance on fresh RPM samples⁵. Refer to Appendix for details on the dataset, experimental setup, *E2E-WReN*, and additional results.

B. Evaluating Abstract Visual Reasoning Results

We compare our results in both the **reasoning accuracy** and the **disentanglement scores** against the SOTA methods. Both scores are important in the context of interpretable reasoning models, as the reasoning accuracy alone does not necessarily reflect the discovery of the underlying RPM factors. Both scores are shown in Table I.

Reasoning. We report the performance of reasoning accuracy in the column “Reasoning” in Table I. Our proposed model **DAREn**, compared against *Staged-WReN* and *E2E-WReN*, shows an improvement of $\sim 2-17\%$ and $\sim 0-2\%$ respectively. It is seen from Table I, our model outperforms the prior work, i.e. *Staged-WReN* by a margin of $\sim 2-17\%$, especially for datasets with color as a ground truth factor (all excluding *dsprites*). The VAE model **DAREn** can firmly separate color attributes from other factors compared to *Staged-WReN*.

The WReN module is similar for both *E2E-WReN* vs. *Staged-WReN*, where it learns a relational structure by aggregating all pairwise relations on the latent space within the images in \mathcal{M} and between \mathcal{M} and candidates in A .

⁵The state space of all RPM questions is huge e.g. in *shapes3d* has 10^6 factor combinations possible per image and a total of 14 total images for $M=3, A=6$ yielding $\sim 10^{614}$ possible RPM (minus invalid configurations)

Dataset	Model	Reasoning	Disentanglement			
			F-VAE	DCI	MIG	SAP
DSprites	<i>Staged-WReN</i>	97.4 \pm 4.2	74.4 \pm 7.3	52.9 \pm 10.5	28.7 \pm 11.5	4.0 \pm 1.4
	<i>E2E-WReN</i>	99.6 \pm 0.5	77.6 \pm 5.0	58.1 \pm 8.0	38.2 \pm 7.7	6.0 \pm 2.2
	DAReN	99.3 \pm 0.5	79.2 \pm 6.2	59.0 \pm 6.4	39.0 \pm 0.0	6.0 \pm 2.0
Mod Dsprites	<i>Staged-WReN</i>	80.0*	44.0 \pm 10.6	31.2 \pm 7.6	13.8 \pm 7.1	6.4 \pm 2.6
	<i>E2E-WReN</i>	85.7 \pm 11.4	65.1 \pm 10.6	43.0 \pm 6.9	26.1 \pm 9.1	8.3 \pm 3.3
	DAReN	86.5 \pm 10.4	77.0 \pm 13.2	50.1 \pm 11.3	34.9 \pm 12.4	12.6 \pm 4.8
Shapes3D	<i>Staged-WReN</i>	90.0*	84.5 \pm 8.7	73.9 \pm 9.0	44.6 \pm 8.8	6.3 \pm 2.9
	<i>E2E-WReN</i>	98.3 \pm 2.0	91.3 \pm 6.5	79.1 \pm 7.7	54.9 \pm 15.7	8.4 \pm 3.8
	DAReN	99.2 \pm 0.8	98.4 \pm 3.2	91.6 \pm 4.7	68.8 \pm 17.5	17.2 \pm 4.8
Realistic	<i>Staged-WReN</i>	55.5 \pm 8.1	45.0 \pm 5.5	37.4 \pm 4.6	22.7 \pm 7.7	9.8 \pm 2.6
	<i>E2E-WReN</i>	72.7 \pm 7.5	55.3 \pm 6.1	42.5 \pm 6.4	29.7 \pm 8.1	12.8 \pm 2.9
	DAReN	73.5 \pm 6.5	75.8 \pm 8.6	50.6 \pm 5.9	36.1 \pm 8.2	19.3 \pm 5.2
Real	<i>Staged-WReN</i>	61.6 \pm 9.4	57.8 \pm 7.5	46.1 \pm 2.5	31.2 \pm 6.1	14.4 \pm 4.0
	<i>E2E-WReN</i>	72.2 \pm 8.8	65.0 \pm 7.3	48.0 \pm 3.5	34.3 \pm 7.0	18.2 \pm 4.4
	DAReN	74.3 \pm 9.9	75.8 \pm 9.7	51.8 \pm 4.9	37.0 \pm 8.1	20.8 \pm 5.3
Toy	<i>Staged-WReN</i>	64.2 \pm 13.3	49.2 \pm 4.1	43.0 \pm 2.5	29.7 \pm 7.0	10.6 \pm 2.4
	<i>E2E-WReN</i>	80.8 \pm 3.5	58.6 \pm 4.2	48.0 \pm 2.9	37.8 \pm 7.9	13.7 \pm 2.9
	DAReN	81.5 \pm 6.8	75.3 \pm 15.4	52.8 \pm 6.8	35.1 \pm 9.6	18.7 \pm 5.5

TABLE I: Performance (mean \pm variance) of **Reasoning** accuracy and four widely used benchmark **Disentanglement Metrics** on the six benchmark datasets. Note: higher score implies better result. The best score for each dataset among the competing models are shown in **bold red** and second-best in **blue**. (Note: * values are taken from [12].)

However, a joint optimization of reasoning + representation (*E2E-WReN*) learns to solve reasoning task better than *Staged-WReN*. Despite the improvement via joint optimization, *WReN* performance is still sub-optimal in learning the underlying reasoning patterns. For each choice filled RPM, the pairwise relation tensor ($6 \times 9 \times 9$) contains intra-pairwise relations formed within \mathcal{M} ($: \times 8 \times 8$) and rest are inter-pairwise relations between \mathcal{M} and candidates in \mathcal{A} . The intra-pairwise relations remain invariant across all six choices. Only the inter-pairwise score between \mathcal{M} and candidates in \mathcal{A} play a key role in inferring the relationship. We verify by extracting the output of edge MLP, i.e., 9×9 feature representations (\mathbb{R}^d), where d is 256 or 512, and computing the L2-norm on these feature vectors. The features of inter pairwise relations given to MLP determine the correct answer. The above is verified on both the trained networks (*Staged-WReN* and *E2E-WReN*) over all the datasets. *DAReN* avoids forming redundant relations; instead, it works by matching the attributes to find the correct row that satisfies the rule in the top two rows. Our results on these datasets provide evidence of a stronger affinity between reasoning and disentanglement (discussed in the section below), which results from jointly learning both tasks.

In Figure 5, we present qualitative analysis of *shapes3d* and modified *dsprites*. The quality of the reconstructed images confirms that the learned distribution correctly captured the image content. In the right column, we present the distribution of per attribute accuracy over the hyperparameter sweep. The performance of object color in modified *dsprites* is sensitive to hyperparameter changes which is evident from large variance. We also see low performance for object shape due to its discrete nature; since our current latent representation is modeled towards real values, it fails to handle discrete representation.

Disentangling. In Table I, “Disentanglement”, we report the

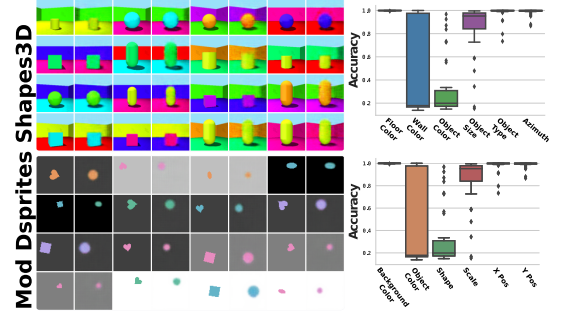


Fig. 5: Top: **Shapes3D**, Bottom: **Mod Dsprites**. In the order of left to right, Reconstructions from *DAReN* (representative samples of median reconstruction error), odd columns show real samples and even columns their reconstruct. Distribution of reasoning performance per generative attribute over all 35 trained models. Expected prior KL-divergence for individual dimensions (left plot represents the best performing model, right plot represents the lowest performing model).

disentanglement scores of trained models on four widely used evaluation metrics namely, the Factor-VAE metric [30], DCI [36], MIG [35], and SAP-Score [37]. *DAReN* improves the reasoning performance and also strongly disentangles the latent vector, in contrast to both *Staged-WReN* and *E2E-WReN*. One primary reason for significant improvements by *DAReN* compared to *Staged-WReN* and even *E2E-WReN* is due to the extraction of the K underlying generative factors and the averaging strategy over the least varying index in K . Generally, in an unsupervised training process, weak signals from the true generative factors often leak into nuisance factors. However, *DAReN* avoids such infusion of nuisance factors by separating o from n .

V. CONCLUSION

We proposed the *GM-RPM* prior and an accompanying learning framework, *DAReN*, to exploit the weak inductive bias present in RPM for visual reasoning. *GM-RPM* provides a backdoor guide on the constraints that can be exploited to solve RPM-based reasoning tasks. To this end, we lifted the emerging evidence of dependency between disentanglement and reasoning [12] one step further by showing that joint end-to-end learning with the appropriate inductive bias can lead to effective simultaneous representation and reasoning models. *DAReN* achieves state-of-the-art results on both the reasoning and the disentanglement metrics. In addition, *DAReN* offers the added flexibility of using arbitrary state-of-the-art factor inference approaches based on ELBO-like objectives to infer and learn the representation needed for accurate reasoning. Our results show evidence of a strong correlation between learning disentangled representation and solving the reasoning tasks. As such, *GR-RPM* and *DAReN* offer a general framework for research in joint learning of representation and reasoning.

REFERENCES

- [1] P. A. Carpenter, M. A. Just, and P. Shell, "What one intelligence test measures: a theoretical account of the processing in the raven progressive matrices test." *Psychological review*, vol. 97, no. 3, p. 404, 1990.
- [2] J. C. Raven, "Standardization of progressive matrices, 1938." *British Journal of Medical Psychology*, 1941.
- [3] J. C. Raven and J. H. Court, *Raven's progressive matrices and vocabulary scales*. Oxford psychologists Press Oxford, England, 1998.
- [4] B. Klein, J. Raven, and S. Fodor, "Scrambled adaptive matrices (sam)—a new test of eductive ability," *Psychological Test and Assessment Modeling*, vol. 60, no. 4, p. 451, 2018.
- [5] D. Hoshen and M. Werman, "Iq of neural networks," *arXiv preprint arXiv:1710.01692*, 2017.
- [6] D. R. Little, S. Lewandowsky, and T. L. Griffiths, "A bayesian model of rule induction in raven's progressive matrices," in *Proceedings of the Annual Meeting of the Cognitive Science Society*, vol. 34, no. 34, 2012.
- [7] A. Lovett and K. Forbus, "Modeling visual problem solving as analogical reasoning," *Psychological review*, vol. 124, no. 1, p. 60, 2017.
- [8] A. Lovett, K. Forbus, and J. Usher, "A structure-mapping model of raven's progressive matrices," in *Proceedings of the Annual Meeting of the Cognitive Science Society*, vol. 32, no. 32, 2010.
- [9] A. Lovett, E. Tomai, K. Forbus, and J. Usher, "Solving geometric analogy problems through two-stage analogical mapping," *Cognitive science*, vol. 33, no. 7, pp. 1192–1231, 2009.
- [10] S. Bringsjord and B. Schimanski, "What is artificial intelligence? psychometric ai as an answer," in *IJCAI*. Citeseer, 2003, pp. 887–893.
- [11] A. Lovett, K. Forbus, and J. Usher, "Analogy with qualitative spatial representations can simulate solving raven's progressive matrices," in *Proceedings of the Annual Meeting of the Cognitive Science Society*, vol. 29, no. 29, 2007.
- [12] S. van Steenkiste, F. Locatello, J. Schmidhuber, and O. Bachem, "Are disentangled representations helpful for abstract visual reasoning?" in *Advances in Neural Information Processing Systems*, 2019, pp. 14 245–14 258.
- [13] D. Barrett, F. Hill, A. Santoro, A. Morcos, and T. Lillicrap, "Measuring abstract reasoning in neural networks," in *International Conference on Machine Learning*, 2018, pp. 511–520.
- [14] C. Zhang, F. Gao, B. Jia, Y. Zhu, and S.-C. Zhu, "Raven: A dataset for relational and analogical visual reasoning," in *Proceedings of the IEEE Conference on Computer Vision and Pattern Recognition*, 2019, pp. 5317–5327.
- [15] X. Steenbrugge, T. Verbelen, S. Leroux, and B. Dhoedt, "Improving generalization for abstract reasoning tasks using disentangled feature representations," in *NeurIPS2018, part of 32nd Conference on Neural Information Processing Systems*, 2018, pp. 1–8.
- [16] Y. LeCun, B. Boser, J. S. Denker, D. Henderson, R. E. Howard, W. Hubbard, and L. D. Jackel, "Backpropagation applied to handwritten zip code recognition," *Neural computation*, vol. 1, no. 4, pp. 541–551, 1989.
- [17] K. He, X. Zhang, S. Ren, and J. Sun, "Deep residual learning for image recognition," in *Proceedings of the IEEE Conference on Computer Vision and Pattern Recognition*, 2016, pp. 770–778.
- [18] Y. Bengio, A. Courville, and P. Vincent, "Representation learning: A review and new perspectives," *IEEE transactions on pattern analysis and machine intelligence*, vol. 35, no. 8, pp. 1798–1828, 2013.
- [19] K. Ridgeway, "A survey of inductive biases for factorial representation-learning," *arXiv preprint arXiv:1612.05299*, 2016.
- [20] F. Locatello, S. Bauer, M. Lucic, G. Raetsch, S. Gelly, B. Schölkopf, and O. Bachem, "Challenging common assumptions in the unsupervised learning of disentangled representations," in *Proceedings of the 36th International Conference on Machine Learning*, ser. Proceedings of Machine Learning Research, K. Chaudhuri and R. Salakhutdinov, Eds., vol. 97. PMLR, 09–15 Jun 2019, pp. 4114–4124. [Online]. Available: <https://proceedings.mlr.press/v97/locatello19a.html>
- [21] D. P. Kingma, S. Mohamed, D. J. Rezende, and M. Welling, "Semi-supervised learning with deep generative models," in *Advances in Neural Information Processing Systems*, 2014, pp. 3581–3589.
- [22] D. Bouchacourt, R. Tomioka, and S. Nowozin, "Multi-level variational autoencoder: Learning disentangled representations from grouped observations," in *Thirty-Second AAAI Conference on Artificial Intelligence*, 2018.
- [23] J. Wang, Y. Song, T. Leung, C. Rosenberg, J. Wang, J. Philbin, B. Chen, and Y. Wu, "Learning fine-grained image similarity with deep ranking," in *Proceedings of the IEEE Conference on Computer Vision and Pattern Recognition*, 2014, pp. 1386–1393.
- [24] K. McGregor and A. Goel, "Confident reasoning on raven's progressive matrices tests," in *Twenty-Eighth AAAI Conference on Artificial Intelligence*, 2014.
- [25] C. S. Mekik, R. Sun, and D. Y. Dai, "Similarity-based reasoning, raven's matrices, and general intelligence," in *IJCAI*, 2018, pp. 1576–1582.
- [26] K. Wang and Z. Su, "Automatic generation of raven's progressive matrices," in *Twenty-Fourth International Joint Conference on Artificial Intelligence*, 2015.
- [27] S. Hu, Y. Ma, X. Liu, Y. Wei, and S. Bai, "Hierarchical rule induction network for abstract visual reasoning," *arXiv preprint arXiv:2002.06838*, vol. 2, no. 4, 2020.
- [28] Y. Benny, N. Pekar, and L. Wolf, "Scale-localized abstract reasoning," in *Proceedings of the IEEE/CVF Conference on Computer Vision and Pattern Recognition*, 2021, pp. 12 557–12 565.
- [29] I. Higgins, L. Matthey, A. Pal, C. P. Burgess, X. Glorot, M. M. Botvinick, S. Mohamed, and A. Lerchner, "beta-vae: Learning basic visual concepts with a constrained variational framework," in *International Conference on Learning Representations*, 2017.
- [30] H. Kim and A. Mnih, "Disentangling by factorising," in *International Conference on Machine Learning*, 2018, pp. 2649–2658.
- [31] M. Kim, Y. Wang, P. Sahu, and V. Pavlovic, "Bayes-factor-vae: Hierarchical bayesian deep auto-encoder models for factor disentanglement," in *Proceedings of the IEEE/CVF International Conference on Computer Vision*, 2019, pp. 2979–2987.
- [32] M. Kim, P. Sahu, Y. Wang, and V. Pavlovic, "Relevance factor vae: Learning and identifying disentangled factors," *arXiv preprint arXiv:1902.01568*, 2019.
- [33] M. Tschannen, O. Bachem, and M. Lucic, "Recent advances in autoencoder-based representation learning," *arXiv preprint arXiv:1812.05069*, 2018.
- [34] C. P. Burgess, I. Higgins, A. Pal, L. Matthey, N. Watters, G. Desjardins, and A. Lerchner, "Understanding disentangling in β -vae," *arXiv preprint arXiv:1804.03599*, 2018.
- [35] R. T. Q. Chen, X. Li, R. Grosse, and D. Duvenaud, "Isolating sources of disentanglement in variational autoencoders," in *Advances in Neural Information Processing Systems*, 2018.
- [36] C. Eastwood and C. K. Williams, "A framework for the quantitative evaluation of disentangled representations," in *International Conference on Learning Representations*, 2018.
- [37] A. Kumar, P. Sattigeri, and A. Balakrishnan, "Variational inference of disentangled latent concepts from unlabeled observations," in *International Conference on Learning Representations*, 2018.
- [38] F. Locatello, M. Tschannen, S. Bauer, G. Rätsch, B. Schölkopf, and O. Bachem, "Disentangling factors of variations using few labels," in *International Conference on Learning Representations*, 2019.
- [39] P. Sorrenson, C. Rother, and U. Köthe, "Disentanglement by nonlinear ica with general incompressible-flow networks (gin)," *arXiv preprint arXiv:2001.04872*, 2020.
- [40] I. Khemakhem, D. Kingma, R. Monti, and A. Hyvarinen, "Variational autoencoders and nonlinear ica: A unifying framework," in *International Conference on Artificial Intelligence and Statistics*. PMLR, 2020, pp. 2207–2217.
- [41] F. Locatello, B. Poole, G. Rätsch, B. Schölkopf, O. Bachem, and M. Tschannen, "Weakly-supervised disentanglement without compromises," in *International Conference on Machine Learning*. PMLR, 2020, pp. 6348–6359.
- [42] H. Hosoya, "Group-based learning of disentangled representations with generalizability for novel contents," *arXiv preprint arXiv:1809.02383*, 2018.
- [43] R. Shu, Y. Chen, A. Kumar, S. Ermon, and B. Poole, "Weakly supervised disentanglement with guarantees," in *International Conference on Learning Representations*, 2019.
- [44] D. P. Kingma and M. Welling, "Auto-encoding variational bayes," *arXiv preprint arXiv:1312.6114*, 2013.
- [45] N. Srivastava, G. Hinton, A. Krizhevsky, I. Sutskever, and R. Salakhutdinov, "Dropout: a simple way to prevent neural networks from overfitting," *The journal of machine learning research*, vol. 15, no. 1, pp. 1929–1958, 2014.

- [46] L. Matthey, I. Higgins, D. Hassabis, and A. Lerchner, “dsprites: Disentanglement testing sprites dataset,” *URL https://github.com/deepmind/dsprites-dataset/*. [Accessed on: 2018-05-08], 2017.
- [47] M. W. Gondal, M. Wuthrich, D. Miladinovic, F. Locatello, M. Breidt, V. Volchkov, J. Akpo, O. Bachem, B. Schölkopf, and S. Bauer, “On the transfer of inductive bias from simulation to the real world: a new disentanglement dataset,” *Advances in Neural Information Processing Systems*, vol. 32, pp. 15 740–15 751, 2019.
- [48] A. Paszke, S. Gross, F. Massa, A. Lerer, J. Bradbury, G. Chanan, T. Killeen, Z. Lin, N. Gimelshein, L. Antiga, A. Desmaison, A. Kopf, E. Yang, Z. DeVito, M. Raison, A. Tejani, S. Chilamkurthy, B. Steiner, L. Fang, J. Bai, and S. Chintala, “Pytorch: An imperative style, high-performance deep learning library,” in *Advances in Neural Information Processing Systems 32*, H. Wallach, H. Larochelle, A. Beygelzimer, F. d’Alché-Buc, E. Fox, and R. Garnett, Eds. Curran Associates, Inc., 2019, pp. 8024–8035. [Online]. Available: <http://papers.nips.cc/paper/9015-pytorch-an-imperative-style-high-performance-deep-learning-library.pdf>
- [49] D. P. Kingma and J. Ba, “Adam: A method for stochastic optimization,” *arXiv preprint arXiv:1412.6980*, 2014.

APPENDIX

A. Experimental Details

We use the same experimental setup such as the architecture, hyperparameters used in the prior work [12]. Our VAE network architecture is similar to Factor VAE, and the reasoning model is a three-layered MLP ($\psi(\cdot)$) with a ReLU, and a dropout layer [45]. The architecture details for DAREN are depicted in Table II. All our models are implemented in PyTorch [48] and optimized using ADAM optimizer [49], with the following parameters: learning rate of $1e - 4$ for the reasoning + representation network excluding the Discriminator (approximation of TC term in Factor VAE) which is set to $1e - 5$, $\beta_1 = 0.9$, $\beta_2 = 0.999$, $\epsilon = 10^{-8}$. To demonstrate that our approach is less sensitive to the choice of the hyper-parameters (γ), and network initialization, we sweep over 35 different hyper parameter settings of $\gamma \in \{1.0, 10.0, 20.0, 30.0, 40.0, 50.0, 100.0\}$ and initialization seeds $\{1, 2, 3, 4, 5\}$. The image size used in all six datasets is $64 \times 64 \times ch$ pixels, where channels, $ch = 3$ for all datasets except for *dsprites* where it is one. We scaled the pixel intensity to $[0, 1]$. For each model, we use a batch size of 64 during the training process, where each mini-batch consists of generated random instances RPMs.

Staged-WReN used SOTA generative models for disentanglement trained upto 300K to train the relational network for 100K (VAE parameters frozen). The relational network is similar to WReN, composed of two MLPs: edge MLP that learns on all pairwise joined representation for each choice, graph MLP that maps the pairwise all feature vector to a single probability score for each choice. On the other hand for *E2E-WReN*, we trained both the representation (only on Factor VAE) and reasoning model upto 300K. Note: VAE was trained on all factor data and the reasoning network on RPM created by quantized factors similar to [12]⁶.

B. Dataset Details

DSprites. The most commonly used dataset for bench marking disentangling is the *dsprites* dataset [46]. It consists of a

TABLE II: Representation (Encoder, Decoder) and Reasoning Architectures.

Encoder	Decoder
Input: # channels $\times 64 \times 64$	Input \mathbb{R}^{10}
4×4 conv. 32 ReLU. stride 2	FC. 256 ReLU
4×4 conv. 32 ReLU. stride 2	FC. $4 \times 4 \times 64$ ReLU
4×4 conv. 64 ReLU. stride 2	4×4 upconv. 64 ReLU. stride 2
4×4 conv. 64 ReLU. stride 2	4×4 upconv. 32 ReLU. stride 2
FC 256. FC 2×10	4×4 upconv. 32 ReLU. stride 2
	4×4 upconv. #channels. stride 2
Discriminator	Reasoning Network
FC. 1000 leaky ReLU	Input $\mathcal{M}: \mathbb{R}^{8 \times 10}$. $\mathcal{A}: \mathbb{R}^{6 \times 10}$
FC. 1000 leaky ReLU	RN Emb. Size: 54
FC. 1000 leaky ReLU	RN MLP: [512, ReLU,
FC. 1000 leaky ReLU	512, ReLU,
FC. 1000 leaky ReLU	512, ReLU
FC. 2	dropout: 0.5,
	1]

single dsprite (color: white) on a blank background and can be fully described by five generative factors: shape (3 values), position x (32 values), position y (32 values), size (6 values) and orientation (40 values). The total images produced are the Cartesian product of the generative factors i.e., 737,280. Ground truth factor changes in the construction of RPMs: three equally distant values of size (instead of 6), four values of x/y position (instead of 32). We ignore orientation factor as certain objects such as squares and ellipses exhibit rotational symmetries. And no changes to shape.

Modified DSprites. [12] is an extension of *dsprites* dataset that adds a background color (5 values), a color attribute (6 values) to the single dsprite, and excluding the orientation factor. Colors are sampled from a linear HUSL hue space. The total images produced are the Cartesian product of the generative factors, i.e., 552,960. Ground truth factor changes in the construction of RPMs: shape, size, x/y position remains the same as in *dsprites* with two additional color factors.

3D Shapes. “3D Shapes” [30] consists of images of a single 3D object in a room and is fully specified by six generative factors: floor colour (10 values), wall colour (10 values), object colour (10 values), size (8 values), shape (4 values) and rotation (16 values). The total images produced are the Cartesian product of the generative factors, i.e., 480,000. Ground truth factor changes in the construction of RPMs: four equally distant factors for rotation and size (instead of 8 and 16) and no changes to the rest.

MPI3D-(Real, Realistic, Toy). [47] created a recent bench marking robotics dataset for disentanglement across simulated to real-world environments (Toy, Realistic, Real). It consists of images of a sprite on a robotic arm and is fully specified by six generative seven generative factors: object color (6 values), object shape (6 values), object size (2 values), camera height (3 values), background color (3 values), horizontal axis (40 values), vertical axis (40 values). The horizontal and vertical axes are sampled from a uniform distribution, and the other five factors take discrete values. Each dataset

⁶The quantization ensured visually distinguishable factor values for each factor of variation to humans.

contains all possible combinations of the factors that amount to total images in the dataset i.e., 1,036,800. Ground truth factor changes in the construction of RPMs: four equally distant factors for horizontal and vertical axis (instead of 40) and no change to the rest.

Generating RPM Questions. Here we describe the process followed to automatically generate RPM, derived from [12], [26]. The procedure requires access to the ground truth factors of the dataset. The dataset generation process can be divided into three parts: i) determining the rule for a sample instance, ii) placing images satisfying the rule in the matrix, iii) generating incorrect alternatives to form choice panel. We fixed the matrix size as a 3×3 where the bottom right image is removed and placed among five incorrect answers in a randomly chosen location. We also fixed the relation type to constant in a row. This means that the three images present in any matrix row should have at least one object factor constant. In step one of the process, we start by sampling a subset of ground truth factors that we fix across all three rows. Next, we uniformly sample values without replacement for this fixed subset of factors for each row separately. The subset of factors is our underlying rule for this sample, where the values taken by them are constant in a row, and this subset of factors remains fixed across all the rows. Finally, the rest of the factors that are not part of the rule are allowed to take any factor value as long as these values are not the same across the first two rows. This is done to ensure that each of these rows have a different set of constant factors that are not part of the rule. However, the solution to the final row must come from the subset of factors that are constant across the first two rows. Once all the factors are sampled for the 3×3 matrix, the next step is to retrieve corresponding images from the dataset. The final step consists of sampling hard incorrect answers for the sample to form the choice panel. We start by taking the correct answer factors and keep on resampling until it no longer satisfies the underlying rule. This process is repeated five times to generate alternative panels. Finally, the correct answer panel is inserted in this choice list in a random position. Note: The sampled factors are from the list of quantized factors described in Section B. Please refer to Figure 6 for sample instances of abstract visual reasoning tasks on all six datasets.

C. E2E-WReN

For a RPM of size 3×3 , we adopt the same notation used in [12] to represent the matrix without the bottom last element as \mathcal{M} and the image choices with the correct answer as the answer panels A (size = 6 as in prior work).

WReN is evaluated on the embeddings from a deep Convolutional Neural Network (CNN). For each choice image placed at the missing location, WReN forms all pairwise combination among all the nine latent embeddings and outputs a score. The relational network is a non-linear composition of two functions f_ϕ and g_θ which are implemented as multilayer perceptrons (MLPs). The pairwise embeddings generated above are given as an input to g_θ of the relational network. This stage is tasked with inferring relations between object properties for a given

pair, between context and choice panel, and between context panels. The output of g_θ for each pairwise embeddings is aggregated. The aggregated representation for all six choices is given as an input to the f_ϕ function, which outputs the logit score for all the choices and the score with the highest choice is predicted as final output.

D. Additional Results

Below we present the reconstructed samples (Figure 7) using DAREn for different data sets that are representative of the median reconstruction error.

Next, we present the latent traversal of DAREn over all the datasets, where the highlighted latent dimensions mark the presence of a generative factor our model successfully extracted, Figure 8.

Figure 9 displays the expected KL divergence for individual dimensions over all datasets. The left plot refers to the best performing model among all the models trained and the right plot presents the bad model trained. The count of bars in each plot (in best model) is same to the count of generative factors in each dataset which suggests our model minimizes duplicating or entangling more than factors. Finally, Figure 10 displays the distribution of performance for each generative factor in the visual reasoning tasks.

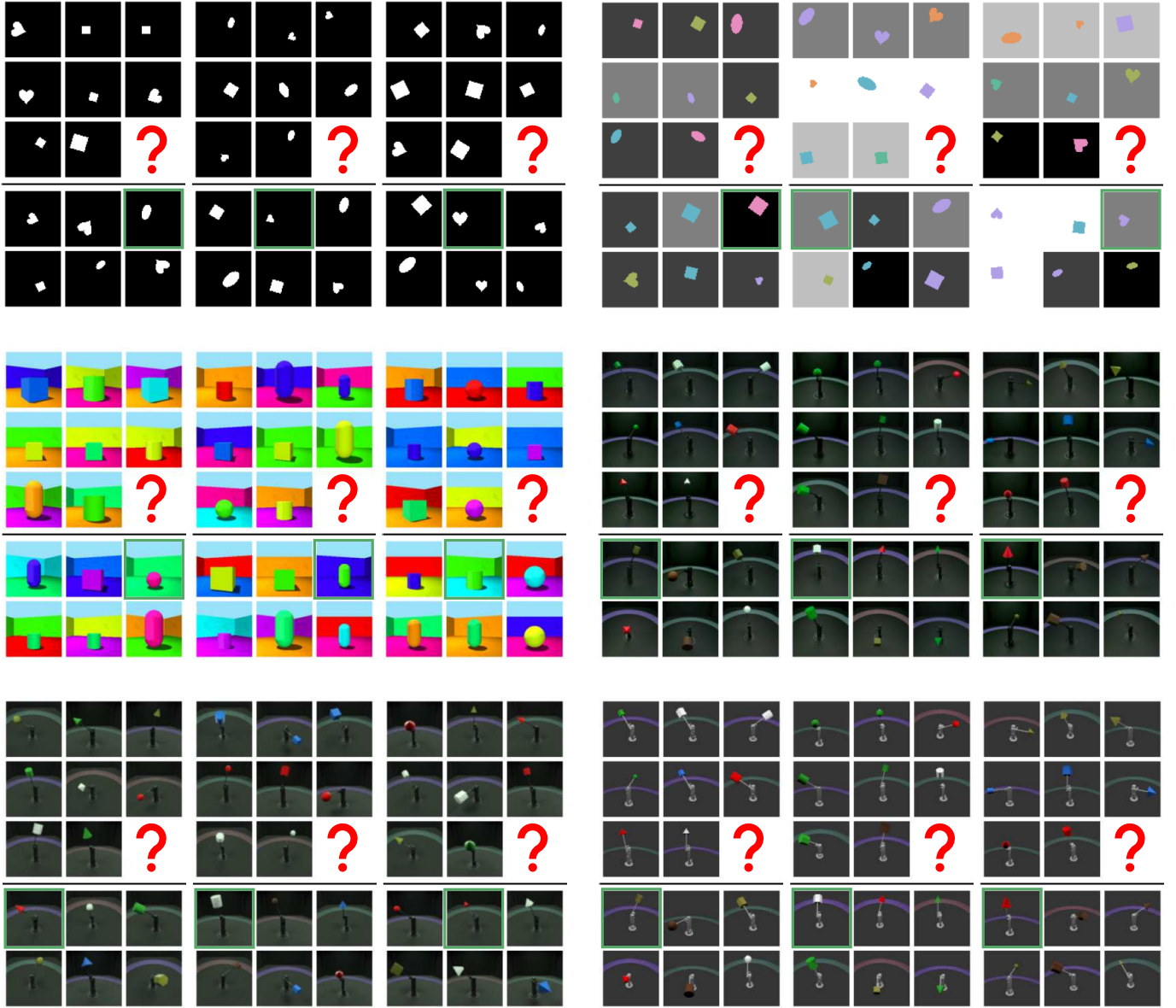


Fig. 6: Sample RPM based Abstract Visual Reasoning Tasks for DSprites, Modified DSprites, Shapes3D, MPI3D Real, MPI3D Realistic, MPI3D Toy. (Order: Left to Right, Top to Bottom)

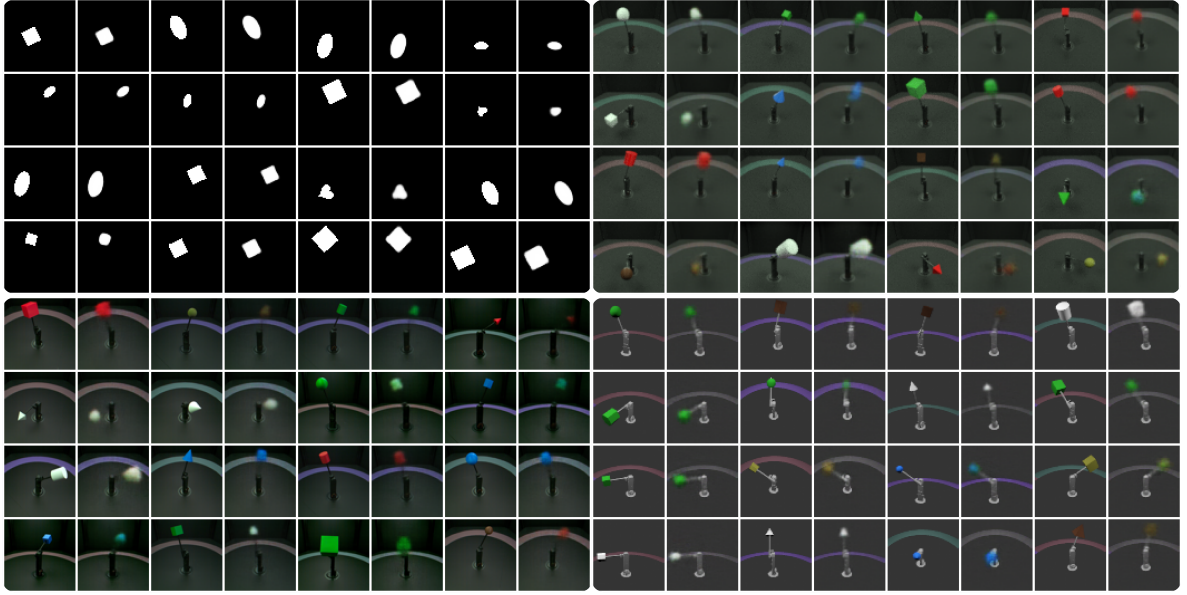


Fig. 7: Ground truth and reconstructions on the remaining four datasets: *dsprites*, *MPI3D-Realistic*, *MPI3D-Real*, *MPI3D-Toy* (Left to Right, Top to Bottom), using trained DAREn at 300K. Odd columns show real samples and even columns their reconstruction.

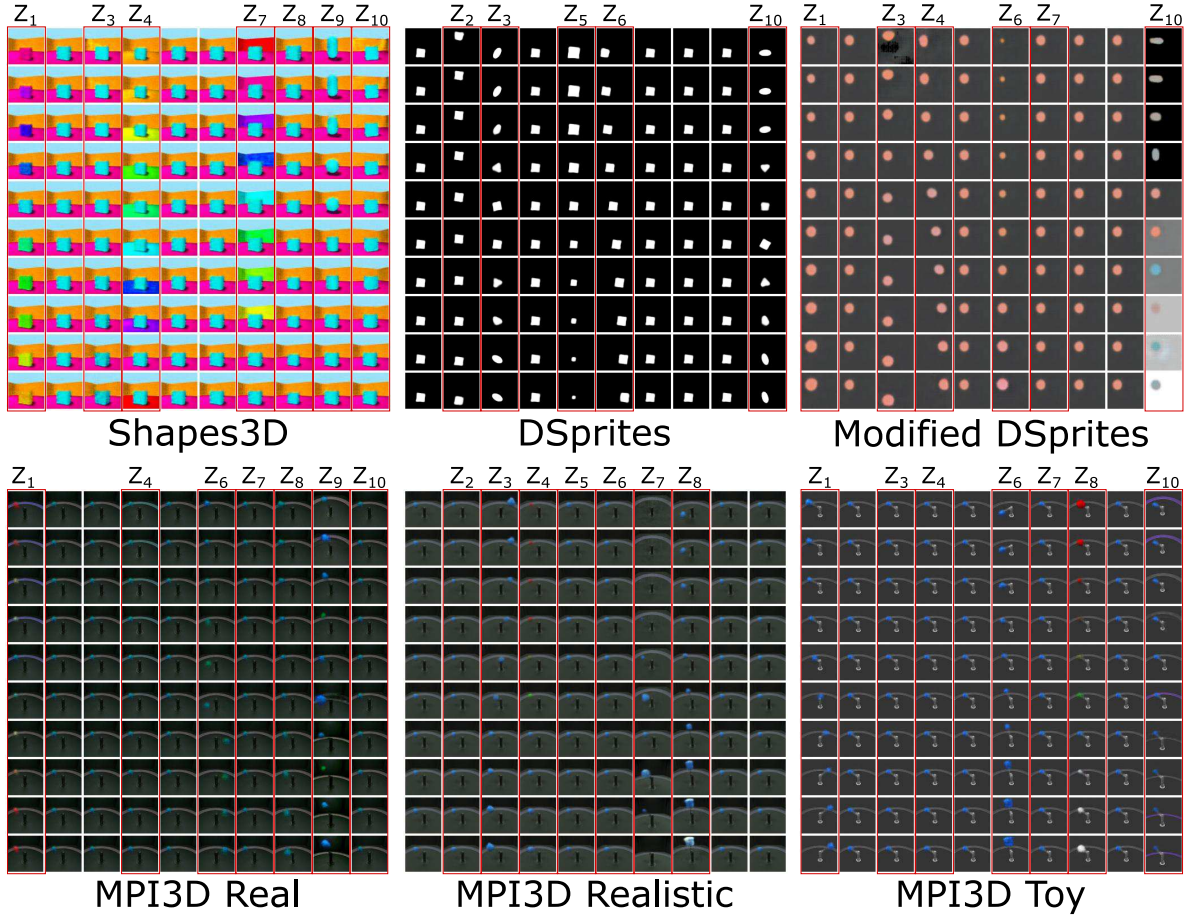


Fig. 8: Latent space traversal of DAREn on all datasets. The visibly evident latent dimensions of variability are highlighted within color boxes where each exactly matches one of the four ground-truth factors. Shapes3D: ($Z_1, Z_3, Z_4, Z_7, Z_8, Z_9, Z_{10}$), DSprites: ($Z_1, Z_3, Z_4, Z_7, Z_8, Z_9, Z_{10}$), Modified DSprites: ($Z_1, Z_3, Z_4, Z_6, Z_7, Z_{10}$), MPI3D Real: ($Z_1, Z_4, Z_6, Z_7, Z_8, Z_9, Z_{10}$), MPI3D Realistic: ($Z_2, Z_3, Z_4, Z_5, Z_6, Z_7, Z_8$), MPI3D Toy: ($Z_1, Z_3, Z_4, Z_6, Z_7, Z_8, Z_{10}$)

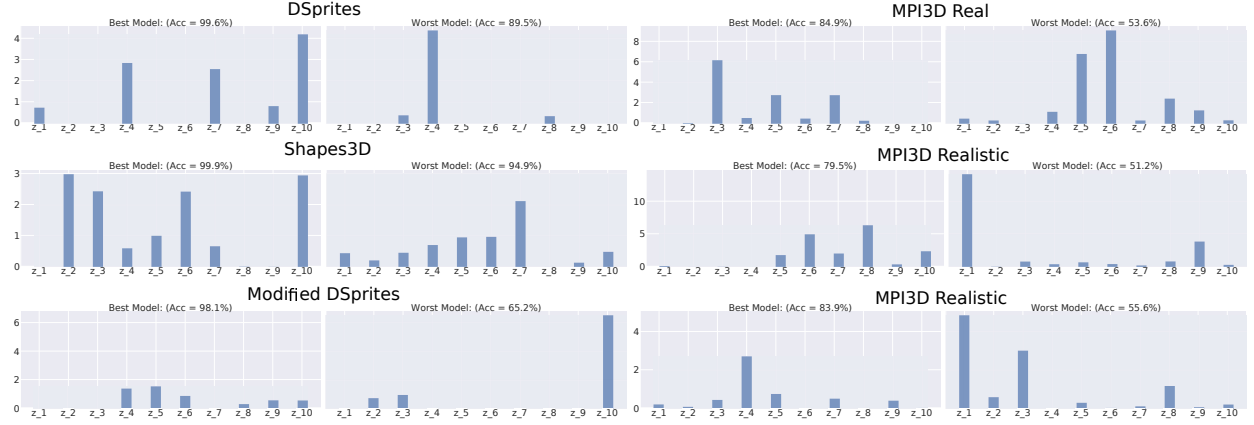


Fig. 9: Expected prior KL divergences for individual dimensions over all datasets. For each dataset, left plot represents the best performing model and right plot represents the lowest performing model over our hyper parameter sweep.

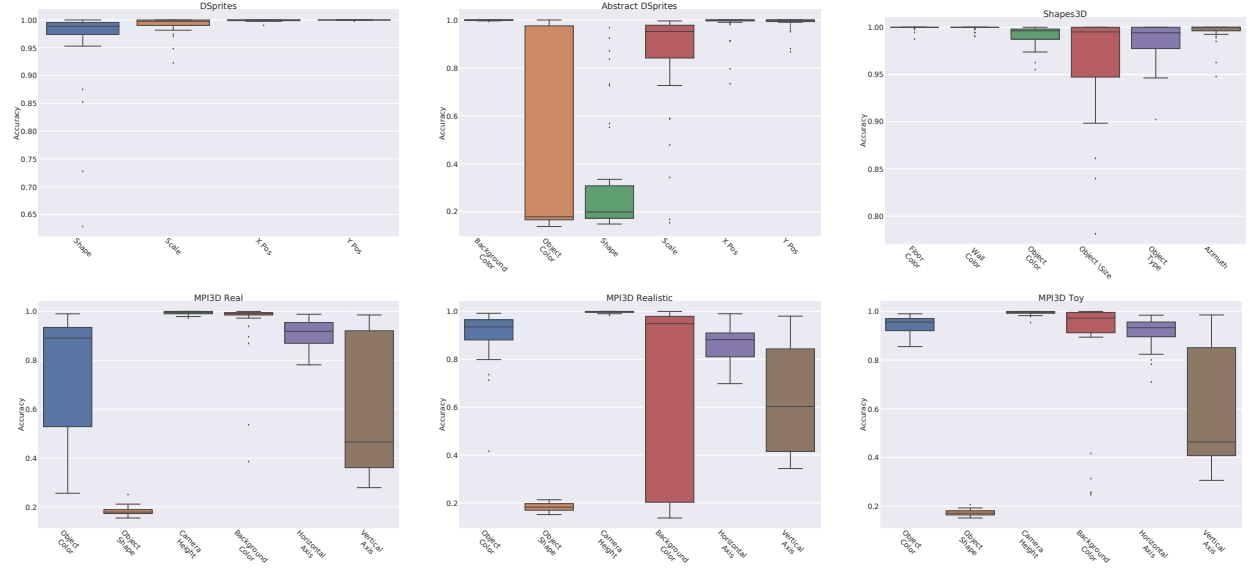


Fig. 10: Distribution of reasoning performance per generative attribute over all models for all datasets. It appears the discrete factor shape is the main reason behind drop in performance.